

7. Y. V. Kuzmin and S. K. Krivonogov, *Geoarchaeology* **9**, 287 (1994).
8. A. G. Pavlov, in *Archaeological Research in Yakutia*, Y. A. Mochanov, Ed. (Nauka, Novosibirsk, Russia, 1992), pp. 20–33.
9. D. H. Krinsley and J. C. Doornkamp, *Atlas of Quartz Sand Surface Textures* (Cambridge Univ. Press, Cambridge, 1973); K. Pye and H. Tsoar, *Aeolian Sand and Sand Dunes* (Unwin Hyman, London, 1990).
10. T. L. Péwé, *U.S. Geol. Surv. Prof. Pap.* 1262 (1983).
11. S. L. Forman, *Quat. Res.* **36**, 19 (1991).
12. M. Frechen, *Quat. Sci. Rev.* **11**, 93 (1992); Y.-C. Lu *et al.*, *Quat. Res.* **28**, 356 (1987); S. C. Packman and R. Grün, *Quat. Sci. Rev.* **11**, 103 (1992); A. G. Wintle, *ibid.* **9**, 385 (1990).
13. Sunlight conditions used were those in Columbus, OH. The TL emission remaining after 8 hours of exposure to a UV-dominated 275-W General Electric sun lamp was used in calculating ages and is a maximum estimate. Ages not reported here but calculated with the use of the residual level determined after 16 hours of sunlight exposure are within two sigma errors of the UV-derived ages (11).
14. The paleodose was determined on the polymineral fine-grained (4 to 11 μm) fraction by the total-bleach method [A. K. Singhvi, Y. P. Sharma, D. P. Agrawal, *Nature* **295**, 313 (1982)] for all samples and for the fine-grained quartz extract from sample OTL487Q. TL measurements were made with Corning 5-58 and Chance-Pilkington HA-3 filters in front of the photomultiplier tube. Samples were preheated at 124°C for 72 hours and subsequently stored at room temperature for 24 hours before analysis. Analyses were completed with a Daybreak 1100 Automated TL systems reader using a Thorn-EMI 9635QB photomultiplier tube. Individual paleodose determinations, at a particular temperature or light exposure time, were determined by means of a nonlinear least-squares routine, based on the Levenberg-Marquardt method, in which inverse-variance weighted data are modeled by a saturating-exponential function [D. J. Huntley; G. W. Berger, S. G. E. Bowman, *Nucl. Tracks Radiat. Meas.* **105**, 279 (1987)]. The highest radiation dose added to the natural TL was at least five times the calculated paleodose, resulting in a <20% extrapolation in determining the paleodose. Error estimates were derived for each paleodose from the inverted curvature matrix. The resultant uncertainties in paleodose calculations reflect dispersion in the data and related random errors from modeling the data by a saturating exponential function. A mean paleodose with errors was evaluated for a range of individual paleodose determinations over a broad temperature range, usually between 250° and 400°C, which included at least 80% of the measured TL signal and was also the temperature region that exhibited a pronounced plateau in paleodose.
15. We tested all samples for anomalous fading by storing irradiated (1000 to 1100 Gy) natural aliquots for at least 32 days and then comparing the TL signal to that of an unstored aliquot. In addition, two samples (OTL472 and OTL487) were tested for anomalous fading over 6 months. Uniformly, the anomalous fading ratio is between 1.00 and 0.94, which indicates little or no fading within analytical resolution.
16. The uranium and thorium concentrations were determined by thick-source alpha counting, which assumes secular equilibrium in the decay series [D. J. Huntley and A. G. Wintle, *Can. J. Earth Sci.* **18**, 419 (1981)]. The ^{40}K level was calculated from the assayed percent of K_2O by inductively coupled plasma-emission spectrometry at Activation Laboratories, Ancaster, Ontario, Canada. A cosmic ray dose component was added [from J. R. Prescott and J. T. Hutton, *Radiat. Meas.* **23**, 497 (1994)]. A moisture content of $25 \pm 5\%$ was assumed. Alpha efficiency (the A value) was determined as defined by M. J. Aitken and S. G. E. Bowman [*Archaeometry* **17**, 132 (1975)].
17. The TL samples OTL471 and OTL472 were not saturated and increased by 50 and 70%, respectively, above the natural TL level after exposure to about 5.6 kGy of beta dose from a calibrated $^{90}\text{Sr}/^{90}\text{Y}$ source. Nine additive doses to the natural TL between 0.1

and 5.6 kGy yielded increasing TL emissions, modeled by a saturating exponential function. The precision of analyses is high, with quadruplicate measurements of TL emissions made for applied beta doses, with a dispersion of <5% for sample OTL471 and <7.5% for sample OTL472.

18. The majority of artifacts were found on the re-exposed deflation surface overlain by unit IV. However, Mochanov (3) reports that artifacts were recovered under unit III. Current excavations have recovered additional artifacts beneath unit III.
19. D. G. Martinson *et al.*, *Quat. Res.* **27**, 1 (1987).
20. Support for the fieldwork and analysis of samples

was provided by the National Geographic Society (research grant 5036-93), the Advanced Research Program sponsored by the Texas Higher Education Coordinating Board (research grant 010366-010), and NSF (grants ATM 9121944 and DPP-9222972). We thank G. Ingleright, R. Ackerman, R. Bonnichsen, and M. Bonnichsen for assistance and T. Goebel for comments. Finally, we thank Y. Mochanov and S. Fedoseeva for logistical support and hospitality. Both were invited to be co-authors on this paper; however, they declined.

22 October 1996; accepted 14 January 1997

Laser Rapid Prototyping of Photonic Band-Gap Microstructures

Michael C. Wanke,* Olaf Lehmann,† Kurt Müller, Qingzhe Wen,* Michael Stuke

Three-dimensional periodic microstructures of aluminum oxide, which are important for creating photonic band-gap structures (PBGs), were fabricated by laser rapid prototyping by means of laser-induced direct-write deposition from the gas phase. The structures consisted of layers of parallel rods forming a face-centered tetragonal lattice with lattice constants of 66 and 133 micrometers. These structures showed transmission minima centered around 4 terahertz (75 micrometers) and 2 terahertz (150 micrometers), respectively. PBGs will allow precise control of the optical properties of materials, including lasers without threshold.

Three-dimensional (3D) periodic microstructures of aluminum oxide, used to construct PBGs (1), were fabricated by laser rapid prototyping (2) by means of laser-induced direct-write deposition from the gas phase. PBGs are 3D periodic structures that are able to totally reflect electromagnetic radiation in a band of frequencies propagating in any direction (3). They represent a new class of materials that are capable of uniquely controlling radiation. The optical properties of these materials can be tailored in order to fabricate perfect mirrors, lasers without threshold, and unique optical waveguide devices. The lifetime of excited states can be influenced by the ability to modify the density of available optical modes. Difficulties in fabricating small structures have limited demonstrations to the high microwave frequency range, whereas potential applications (4) cover a broad frequency range extending into the visible and even to higher frequencies. The highest documented frequency for a fully 3D PBG is 500 GHz (5), corresponding to a wavelength of 600 μm . Short-wavelength structures (5 μm) have been

fabricated in only two dimensions (6).

With few exceptions, the methods that have been proposed for construction of PBGs with gaps in the millimeter-to-optical range are subtractive, meaning that they start with a block of material and remove sections of it to generate the periodic structure. This is a nontrivial process at high frequencies, and incorporation of specific and well-defined defects, which are crucial for many proposed applications, is very difficult if not impossible. In addition, material can only be removed accurately within a few unit cells from the surface.

Here we describe the construction of 3D PBG materials by laser chemical vapor deposition (LCVD). In this approach, the PBG is built layer by layer directly from the gas phase, in a manner analogous to rapid prototyping. The structure selected by us for the first example represents a compromise between stability for handling, time for fabrication, and the relative amount of material filling the 3D volume (the filling factor). First measurements indicate transmission minima that scale with the period of the structure and have frequencies as high as 4 THz (75 μm). Unlike the techniques mentioned above, LCVD is additive: The structure is built up by deposition, so that desired defects and more complex structures can be incorporated into the underlying periodic structure. With this method, the number of unit cells is limited only by the size of the

Max-Planck-Institut für Biophysikalische Chemie, Post Office Box 2841, D-37018 Göttingen, Germany. E-mail: M. C. Wanke, mwanke@qi.ucsb.edu; M. Stuke, mstuke@gwdg.de

*Present address: Quantum Institute, University of California, Santa Barbara, Santa Barbara, CA 93106, USA.

†Present address: SAP, Neurottstrasse 16, D-69190, Walldorf, Germany.

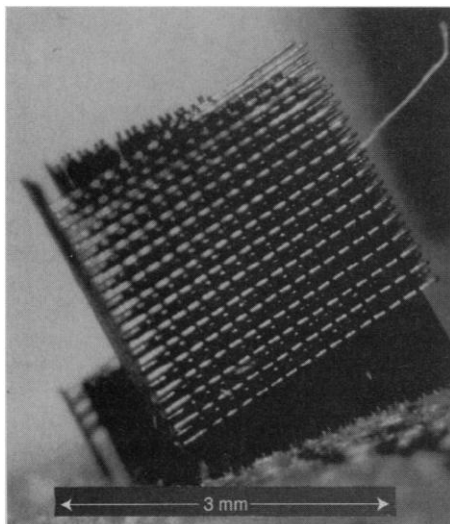


Fig. 1. Three-dimensional PBG structure fabricated by laser rapid prototyping directly from the vapor phase. The periodic structure consists of 15 rows of perpendicularly arranged aluminum oxide rods $40\ \mu\text{m}$ in diameter, with a $133\text{-}\mu\text{m}$ periodicity and rod lengths of $3000\ \mu\text{m}$.

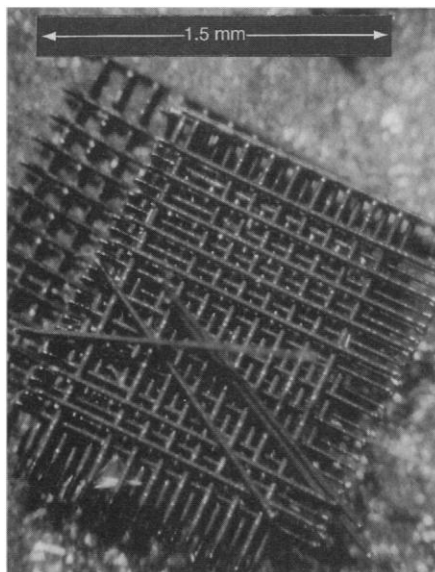


Fig. 2. Partly disassembled aluminum oxide rod structure showing the aluminum oxide rods (diameter, $40\ \mu\text{m}$) and their organization (periodicity, $133\ \mu\text{m}$).

deposition chamber and therefore can be large.

Structures fabricated by LCVD, including rods, microsprings, and microtweezers, have previously been reported and have been constructed from a variety of materials (7–9). In our work, mixtures of oxygen and trimethylamine alane $[(\text{CH}_3)_3\text{N} \cdot \text{AlH}_3]$ or dimethyl-ethyl-amine alane $[(\text{CH}_3)_2\text{C}_2\text{H}_5\text{N} \cdot \text{AlH}_3]$ were used as volatile precursors to grow aluminum oxide (2, 9). Rods $40\ \mu\text{m}$ in diameter were grown at a vertical growth rate of about $60\ \mu\text{m/s}$ with the use of a continuous-wave argon ion laser operating at $488\ \text{nm}$ and about $2\ \text{mW}$, and focused to a spot size about $5\ \mu\text{m}$ in diameter.

We focused on fabricating PBG structures having the same geometry as those made by the Iowa State University Group (5) (that is, planes of parallel rods arranged to form a face-centered tetragonal lattice with a two-rod basis), but we are not limited to this geometry. A set of equally spaced, almost vertical, aluminum oxide rods, aligned in a plane, was grown on a silicon substrate. A plane of horizontal rods was then grown parallel to the plane of vertical rods. As a horizontal rod passed a vertical rod during the growth process, the two grew together, forming a robust connection. As this process was repeated, structures containing 13 planes were constructed, although an arbitrarily large number of layers is possible (Fig. 1). After completion, which can be achieved in less than 1 day, the structures can easily be removed from the substrate, yielding completely free-standing structures. In Fig. 2, a partly disassembled structure reveals the rods and their organization.

Transmission measurements in the far-infrared (FIR) were performed with a Rapid Scan Fourier Transform Spectrometer (Bruker) equipped with a germanium bolometer detector. The samples, whose FIR spectrum is shown (Fig. 3), were $1.25\ \text{mm}$ wide and were placed about $250\ \mu\text{m}$ in front of a brass cone with an aperture $1\ \text{mm}$ in diameter. In this way, the radiation leaking around the structure was minimized. Under the conditions used in our experiment, the surface of the resulting material was black in color, possibly because of an aluminum-rich surface layer, whereas the cores were transparent because laser light could be guided through them. According to preliminary x-ray diffraction studies, the material seems to be amorphous as grown but partially *c* axis-oriented when oxidized. The material, as grown, was opaque in the FIR, which we attribute to the aluminum-rich surface layer. However, when heated above about 800°C in air, the structures become completely oxidized and the FIR transmission increases. The oxidized structures exhibit a shallow gap in the transmission (Fig. 3), which scales with the rod periodicity as expected. The value of the transmission frequency minimum is almost a factor of 2 higher than was expected when the earlier results of the Iowa State University Group were scaled. The overall decay of the transmission at higher frequencies can be attributed to incoherent scattering (10).

In principle, this technique allows the construction of almost any internal structure of a photonic crystal, because each layer is at the surface of the crystal when

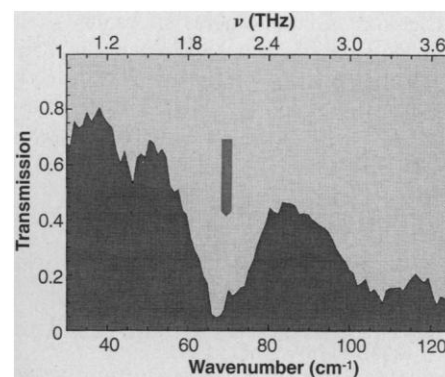


Fig. 3. Vertical incidence FIR transmission spectrum of the PBG structure, showing a transmission frequency (ν) minimum corresponding to $2\ \text{THz}$ ($2 \times 10^{12}\ \text{Hz}$). This is the highest value reported.

grown. Thus, desired internal defects (11) can be incorporated easily. Other advantages offered by this method are the ability to grow around devices (12) that are already present on a wafer. This adds the possibility of incorporating active devices directly into the structures. Material can also be locally doped during growth. Although the structures presented here were made of aluminum oxide, other CVD precursors can be used to grow a large variety of other materials and heterostructures. Rods can also be grown at angles as great as 70° from the laser axis, even with a single laser beam, which makes it possible to grow structures with more complex internal patterns, such as a diamond lattice (Fig. 4).

The structures presented here did not challenge our systems abilities. The overall size of the photonic crystal is only limited by the size of the growth chamber. Individual rods $10\ \mu\text{m}$ in diameter were grown for the full length of the chamber (over $5000\ \mu\text{m}$). The achievable minimum rod diameter is given by the laser focal spot size, and

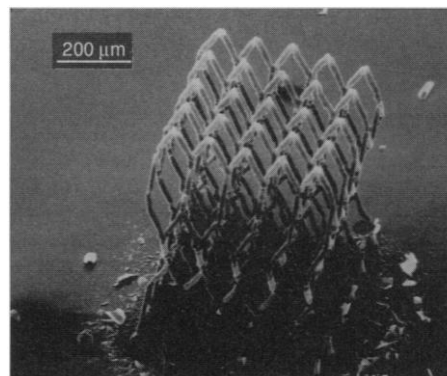


Fig. 4. Scanning electron microscope picture of a laser-written, aluminum oxide, periodic 3D microstructure in the form of a diamond lattice as an alternative demonstrating the flexibility of this laser rapid prototyping method.

therefore submicrometer structures should be possible, especially when photochemically enhanced processes are used instead of purely thermal growth. The latter was used here because it allows a high growth rate (up to 100 $\mu\text{m/s}$).

REFERENCES AND NOTES

1. E. Yablonowitch, *Phys. Rev. Lett.* **58**, 2059 (1987).
2. O. Lehmann and M. Stuke, *Science* **270**, 1644 (1995) and references therein.
3. E. Yablonowitch *et al.*, *Phys. Rev. Lett.* **67**, 3380 (1991) and references therein.
4. Special issues of *J. Opt. Soc. Am.* **B10**, no. 2 (1993) and *J. Mod. Opt.* **41**, 171 (1994); C. M. Soukoulis, Ed., *Photonic Band Gap Materials* (Kluwer Academic, Dordrecht, Netherlands, 1996).
5. E. Özbay *et al.*, *Opt. Lett.* **19**, 1155 (1994). See also other publications from this group.
6. U. Grüning, V. Lehmann, S. Ottow, K. Busch, *Appl. Phys. Lett.* **68**, 747 (1996); A. Rosenberg *et al.*, *Opt.*

- Let.* **21**, 830 (1996).
7. F. T. Wallenberger, *Science* **267**, 1274 (1995) and references therein.
8. M. Boman, H. Westberg, S. Johansson, J.-Å. Schweitz, *Proceedings of the 5th International Workshop on Micro Electro Mechanical Systems*, Trarümünde, Germany, 4 to 7 February 1992 (Institute of Electrical and Electronics Engineers, Piscataway, NJ, 1992).
9. O. Lehmann and M. Stuke, *Mater. Lett.* **21**, 131 (1994).
10. V. N. Bogomolov *et al.*, *Appl. Phys.* **A63**, 617 (1996).
11. E. Özbay and B. Temelkuran, *Appl. Phys. Lett.* **69**, 743 (1996).
12. H. Hirayama, T. Hamano, Y. Aoyagi, *ibid.*, p. 791.
13. We thank U. Biermann (Philips Eindhoven) for support; H. Hahn and his group at the Technische Hochschule (TH) Darmstadt, D. Clark, and Y. Li for x-ray measurements; and Bundesministerium für Bildung, Wissenschaft, Forschung und Technologie (grant 13 N 6159 7), the European Research Office (grant USARDSG-UK), and NSF for financial support.

6 September 1996; accepted 18 December 1996

Low-Temperature Nonoxidative Activation of Methane over *H*-Galloaluminosilicate (MFI) Zeolite

Vasant R. Choudhary,* Anil K. Kinage, Tushar V. Choudhary

Conversion of methane to higher hydrocarbons by its low-temperature activation without forming undesirable carbon oxides is of great scientific and practical importance. Methane can be highly activated, yielding high rates of conversion to higher hydrocarbons and aromatics (10 to 45 percent) at low temperatures (400° to 600°C), by its reaction over *H*-galloaluminosilicate ZSM-5 type (MFI) zeolite in the presence of alkenes or higher alkanes. The methane activation results from its hydrogen-transfer reaction with alkenes.

Methane, the most inert of hydrocarbons, has been extremely difficult to activate for direct conversion to higher hydrocarbons. In the past 10 to 12 years, some success has been achieved by oxidative coupling of methane (OCM) to ethane and ethylene over a number of basic catalysts in the presence or absence of free oxygen (1–4) and over pentasil zeolites with nitrous oxide as the oxidant (5). In the OCM process, the selectivity for higher hydrocarbons is high only at low conversion rates. Moreover, this process involves formation of undesirable products such as CO_2 and CO because of the highly exothermic hydrocarbon combustion reactions, which can also be hazardous. More recently, a dehydrogenative coupling of methane to ethane over active carbon was reported (6). However, the temperature required for methane activation by its dehydrogenative coupling is very high ($\geq 1100^\circ\text{C}$).

Our new approach for obtaining high rates of conversion of methane to higher hydrocarbons, without formation of carbon oxides and at much lower temperatures (400° to 600°C), involves nonoxidative activation of methane by hydrogen-transfer reactions between methane and alkene over *H*-GaAlMFI zeolite. The zeolite is a bifunctional catalyst with strong acid sites (because of the tetrahedral Al and Ga in the zeolite framework) as well as dehydrogenation functions (because of a combination of zeolitic protons and extra framework Ga-oxide species).

To illustrate this approach, we converted methane to higher hydrocarbons (or aromatics) over the zeolite through the addition of C_2 to C_4 alkenes, propane, or *n*-hexane in the feed. The zeolite was prepared and characterized by procedures similar to those in (7). Catalytic reactions were carried out at ambient pressure in a continuous-flow tubular reactor (8, 9). The reactor (internal diameter, 13 mm) was made of quartz. A mixture of N_2 (>99.99%), methane (99.95%), and alkene or higher alkane (>99.5%) was

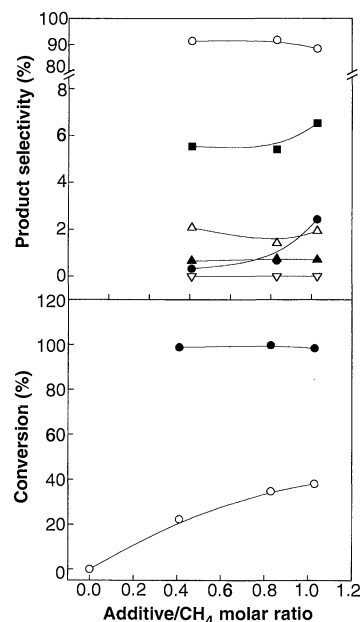


Fig. 1. Effect of the propene/methane molar ratio in feed on the conversion of methane (○) and propene (●) and the selectivity for aromatics (○), ethene (△), ethane (▲), propane (■), C_4 (●), and C_{5+} (▽) aliphatics in the simultaneous aromatization of methane and propene over *H*-GaAlMFI zeolite at 500°C (concentration of methane in feed, 33.3 mol %; space velocity, 6200 $\text{cm}^3 \text{g}^{-1} \text{hour}^{-1}$).

passed over the zeolite catalyst (1 g) for a period of ~5 min at different feed compositions and temperatures. The square pulse technique previously described (9) was used. The space velocity of the feed gas mixtures was measured at 0°C and 1 atm. The conversion and product selectivity data were obtained from the feed and product composition as follows:

Conversion (%)

$$= \frac{\left[\begin{array}{l} \text{weight \% of reactants} \\ \text{in the feed hydrocarbons} \end{array} - \begin{array}{l} \text{weight \% of reactants in the} \\ \text{product hydrocarbons} \end{array} \right]}{\text{weight \% of reactants in} \\ \text{the feed hydrocarbons}} \times 100 \quad (1)$$

Product selectivity (%)

$$= \frac{\left[\begin{array}{l} \text{weight \% of the product} \\ \text{in the hydrocarbon products} \end{array} \right]}{\left[\begin{array}{l} 100 - \text{weight \% of reactants} \\ \text{in the hydrocarbon products} \end{array} \right]} \times 100 \quad (2)$$

The conversion of feed hydrocarbon (or hydrocarbons) to carbon (coke on the catalyst) was found to be ≤ 1 weight %. The carbon and hydrogen balances in the reactions were within 3 to 7%.

Chemical Engineering Division, National Chemical Laboratory, Pune 411 008, India.

*To whom correspondence should be addressed. E-mail: vrc@ncl.ernet.in